Valorization of wipe wastes for the synthesis of microporous carbons and their application in CO_2 capture, gas separation and H_2-storage[☆]

J.A. Cecilia [a,**], E. Vilarrasa-García [b], D.C.S. Azevedo [b], A. Vílchez-Cózar [a], A. Infantes-Molina [a], D. Ballesteros-Plata [a], I. Barroso-Martín [a], E. Rodríguez-Castellón [a,*]

[a] *Departamento de Química Inorgánica, Cristalografía y Mineralogía, Facultad de Ciencias, Universidad de Málaga, 29071 Málaga, Spain*
[b] *GPSA - Grupo de Pesquisa em Separações por Adsorção, Departamento de Engenharia Química, Universidade Federal do Ceará, Campus do Pici, Fortaleza 60455-760, Brazil*

A R T I C L E   I N F O

A B S T R A C T

Wipe wastes have been used as a cellulosic source to synthesize biochars. Prior to the synthesis of the adsorbents by the pyrolysis of wipes wastes, this waste was treated to remove the pathogenic agents. Then, the wipe wastes were pyrolyzed between 500 and 900 °C to obtain biochars, whose microporosity increased proportionally to the pyrolysis temperature, achieving a maximum CO_2-adsorption uptake of 2.53 mmol/g at a pressure of 760 mm of Hg and 25 °C for the biochar pyrolized at 900 °C. The synthesized biochars are also highly selective towards CO_2-adsorption in CO_2/N_2 or CO_2/H_2 mixtures. Hence, these adsorbents have shown a great potential to be used in flue gas treatment and H_2-purification processes. Biochar treatment with KOH further improves microporosity due to chemical activation although the addition of a large amount of KOH leads to excessive microporosity causing a collapse in the pore structure and decreasing CO_2-adsorption capacity.

1. Introduction

Nowadays, the abundant use of wipes and their subsequent disposal by toilet flushing are causing serious problems due to piping blockage in municipal and residential sewer systems because of their accumulation in wastewater treatment plants. This buildup occurs because the pumps, pipes or other sections that process flushable waste in wastewater treatment plants are usually not capable of handling such waste. Disposable wipes have been used in a wide range of applications from make-up removal to sanitary cleaning. The commercial appeal of the wipes is related to their simple use and disposal, in fact wipes are labeled as flushable in many cases.

Currently, the term disposable is becoming quite controversial since these wipes do not have fast enough biodegradation to be efficiently disposed of by the sewage system, causing blockage in wastewater treatment systems.

For example, it is estimated that United States households and companies spent about $2.5 billion on disposal wipes in 2019. However, there are no reliable correlations or statistics on how much disposal wipes are flushed down in toilets, although there are quite a few reports about clogged household plumbing and costly their respective damage to sewer systems and treatment plants caused when the disposal wipes are flushed [1]. The National Association of Clean Water Agencies (NACWA) has pointed out that wipe wastes disposal represents an additional cost of $441 million per year to United States clean water utilities [1]. Likewise, the European Union has indicated that the costs related to the management of wastes coming from the disposal wipes range between €3 and €10 per person per year. Regarding to the maintenance and repair of the sewer facilities, European Union estimated that the cost related to waste disposal for sewage debris coming from wastewater treatment plants amounts from €500 to €1000 million per year. In addition, coastal populations generally assume the costs of removing these wastes from the beaches [2].

Considering the high costs of the wastewater treatment system, it is necessary to carry out awareness programs for the proper disposal of wipes. However, a challenging task is also related to the treatment of these wastes, which currently lacks commercial value, and this is a clear drive to its valorization.

The wipes are made up of a cellulose base with a wide range of additives, which are essentially composed of water and surfactants, oils, emulsions, vegetable ingredients or preservatives to prevent mold formation. Other cellulose-rich materials have been treated to obtain a wide range of carbon-based products of commercial value by physical and chemical processes [3,4]. Among these products, biochar is a material that can be synthesized from cellulose waste by a thermochemical activation in the absence of an oxidizing medium [5,6], leading to microporous materials with many uses and applications in several fields such as catalysis, electrochemistry, gas storage and separation, adsorption and purification or medical applications among others [7–10].

One of the most studied applications is their use in adsorption and gas separation processes due to their narrow pore size distribution that allows hosting small molecules in their structure [11,12]. Among these small molecules, the studies of CO_2-capture have been a challenge for the scientific community since the anthropogenic emissions of this gas have been causing severe damage to the planet because of the aggravation of the denoted as greenhouse effect. Thus, the increase in CO_2-anthropogenic levels is related to a progressive global warming, leading to drastic climate events such as the melting of the poles, prolonged droughts and torrential rains. All this has affected both the fauna and flora of the planet, causing famine and loss of biodiversity.

Under these premises, the most mature technology to minimize CO_2-levels is its capture, transport and storage or utilization [13–15]. Focusing on the CO_2-capture and storage concept (CCS), the CO_2-capture is the most expensive step, accounting for up to 90% of CCS [13]. Therefore, an important challenge is to obtain economically competitive adsorbents with high CO_2-adsorption capacity.

In this context, several fibrous phyllosilicates such as sepiolite and palygorskite have shown a good adsorption capacity by the existence of nanocavities in their structure in such a way that the trapping of CO_2 molecules is possible [16,17]. In the same way, some zeolites are materials that can be synthesized relatively easily (e.g., from fly ashes) with low-cost chemicals [18–20]. Other adsorbents with high porosity and narrow pore size distribution are biochars and activated carbons. These adsorbents are formed by a high temperature pyrolytic treatment where a hydrocarbon structure is transformed into a microporous material with a carbon-based skeleton. For an economically sustainable process, the hydrocarbon source is usually an agricultural waste (seeds or shells) [12] , [21–25], which have a high lignocellulose content. Considering these premises, it is expected that other cellulosic sources, such as disposable wipes, can give rise to carbonaceous materials with good textural properties and an appreciable capacity to capture CO_2. On the other hand, the most outstanding benefit of this study is the valorization of this waste, which clogs pipes and collectors and causes an increase in costs, to give rise to a compound with high added value for environmental-friendly uses.

2. Materials and methods

2.1. Synthesis of the adsorbents

Wipe waste was collected from a wastewater treatment plant of municipal water company of Málaga (EMASA). These residues were obtained from purification collectors and dried in the sun by company operators.

To eliminate pathogenic compounds, the wipe was treated with a NaClO solution (20% vol.) for 24h. After that, the wipe was washed to remove excess NaClO and dried at 80 °C for 12h. Finally, the disinfected wipes were cut to allow the pyrolytic treatment into the oven.

For the pyrolysis treatment, 2 g of wipe waste was placed in an Al_2O_3 crucible. Then, each sample was treated between 500 and 900 °C at a ramp of 5 °C/min using N_2-flow of 50 mL/min, maintaining the selected pyrolysis temperature for 2h. Then, the obtained biochar was cooled down under N_2-flow under the similar flow rate until room temperature. These biochars were labeled as W-X, where X indicates the pyrolysis temperature.

To improve the textural properties of the biochars, they were chemically activated by adding several proportions of KOH in order to obtain activated carbons. Thus, the first step was the synthesis of biochar at 500 °C according to the procedure described previously. In the activation step, 2 g of the biochar synthesized at 500 °C were physically mixed with different proportions of KOH (20–60 wt%) and then the biochars were pyrolyzed at 900 °C at a heating ramp of 5 °C/min using a N_2-flow rate of 50 mL/min, maintaining the final temperature for 2h. Then, the samples were cooled under the same N_2-flow until room temperature. In a final step, the activated carbons were washed to remove the remaining KOH. The samples were labeled as W-900-YKOH, where Y indicated the KOH concentration in wt.% used to synthesize of the activated carbons.

2.2. Characterization techniques

Raman spectra were performed in a micro-Raman JASCO NRS-5100 equipment. This apparatus combines a confocal microscope with dispersive Raman spectrometer and a confocal microscope, which was equipped with DSF (Dual Spatial Filter) to optimize confocally. This equipment minimizes optical aberrations, improving resolution up to 0.4 cm^{-1}. The calibration of the laser lines was performed with respect to silicon while the detection was attained through a high-resolution Charge Coupled Device (CCD). All experiments were carried out in a Nd:YAG laser with a wavelength of 532 nm, an acquisition time of 10 s (10 accumulations), a power between 2.4 mW and 4.6 mW and an objective of 100×.

^{13}C magic angle spinning nuclear magnetic resonance (MAS-NMR) spectra were collected at room temperature in an AVANCEIII HD 600 (Bruker AXS) equipment, which was equipped with a triple resonance CP-MAS probe of 3.2 mm at a spinning rate of 15 kHz. The magnetic field was 14.1 T, which corresponds to a ^{13}C resonance frequency of 150.91 MHz. The ^{13}C chemical shifts were referenced to adamantane. ^{13}C MAS NMR spectra were recorded with 7-s delay with 1H decoupling (^{13}C Hpdec with tppm15 decoupling sequence for C) and summing up 5000 scans.

X-ray photoelectron spectra were recorded with a Physical Electronic PHI 5700 spectrometer, which is equipped with a Mg Kα X-ray excitation source (15 kV, 300 W, hν = 1253.6 eV) and an Electronics 80–365B multichannel hemispherical electron analyzer. All spectra were registered by a concentric hemispherical analyzer in a constant energy mode of 29.35 eV, using a 720 μm diameter analysis area. The pressure in the analysis chamber was maintained below 5×10^{-6} Pa. Binding energies values were estimated to an accuracy of ±0.1 eV, using the adventitious carbon C 1s signal at 284.8 eV as reference to counteract the charge effect. A PHI ACCESS ESCA-F V6 software was utilized for data acquisition and analysis. A Shirley-type background was subtracted from the original spectra. The recorded spectra were always analyzed with Gauss-Lorentz curves, to determine the binding energy of the atomic levels of the different elements more precisely.

The textural properties of the biochars and activated carbons was estimated in a Micromeritics 2420 equipment. Samples were previously degassed (120 °C and 10^{-5} bar for 12h). The specific surface area and the micropore volume of the adsorbents were determined by N$_2$-adsorption at −196 °C and CO$_2$-adsorption at 0 °C. The corresponding surface area (SDA) and the micropore volume (V$_{micro}$) values were determined by the Dubinin-Radushkevich equation. The density of the biochar samples was analyzed on a gas pycnometer AccuPyc II 1340 supplied by Micromeritics Instrument Corporation.

The morphology of the wipes and the biochars synthesized at different pyrolysis temperatures were assessed using a scanning electron microscope (SEM) with JEOL SM-6490 LV equipment. The samples for SEM observation were gold-sputtered to avoid charging of the surface.

2.3. Adsorption experiments and equilibrium model

The CO$_2$-adsorption isotherms were carried out between 0 and 45 °C. These measurements were carried out in a Micromeritics 2420 equipment. Prior to the analysis, the samples were outgassed at 150 °C and 10^{-5} bar overnight.

The CO$_2$-adsorption isotherms were adjusted using the SIPS model, which is defined by the following equation (Eq. 1):

$$q = \frac{q_m(bP)^n}{1 + (bP)^n} \tag{1}$$

where q is the amount adsorbed (mmol/g) when the equilibrium conditions are reached at a given pressure and temperature and q_m is the maximum amount adsorbed (mmol/g), respectively. The b-parameter (mm Hg^{-1}) is associated to the adsorbate-adsorbent affinity while the n-parameter is related to the heterogeneity of the adsorbent on its surface. When n-parameter is close to the unity, the surface of the adsorbent can be considered as homogeneous so that the SIPS equation model can be reduced to the Langmuir model.

The isosteric heats of adsorption (q_{ist}) were determined through the adsorption data collected at 0, 25 and 45 °C applying the Clausius Clapeyron equation (Eq. 2).
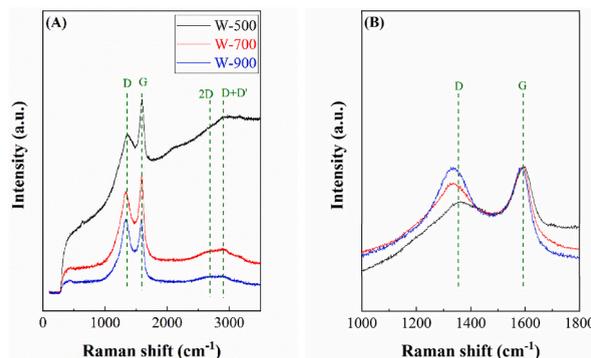

Fig. 1. Raman spectra of the biochars synthesized at different temperatures (A) and normalized Raman spectra (B).

$$\ln p = -\frac{(q_{ist})}{R} \times \frac{1}{T} \tag{2}$$

where q_{ist} is the isosteric heat of adsorption (kJ/mol) and R is the ideal gas law constant.

3. Results and discussion

3.1. Characterization

The biochars obtained after the pyrolytic treatment of wipe wastes were studied by Raman spectroscopy (Fig. 1A). All samples show two well-defined bands located at 1332 and 1591 cm^{-1}, which are assigned to the disorder (D) and graphite (G) bands, respectively [26,27]. The presence of the D band is attributed to the A$_{1g}$ vibrational mode. This signal is an in-plane breathing type of vibration, suggesting the formation of a disordered graphitic lattice, so this signal is related to the drop of hexagonal symmetry in the graphite framework because this signal is inactive for highly oriented and large graphite crystals [28]. In the case of the G band, this signal assigned to the Raman active E$_{2g}$ in-plane vibration mode. This vibration is typical of the ideal graphite lattice [28]. From the intensity ratio of D and G bands (I$_D$/I$_G$) (Fig. 1B), it is possible to infer about the morphology and nature of the biochar obtained after the pyrolytic treatment of the wipes waste. The increase in temperature in the pyrolytic treatment provokes an increase of the I$_D$/I$_G$ ratio from 0.6 for W-500 sample to 1.3 for W-900 sample. This suggests that an increase in the size of the sp^2 clusters, which is related to the formation of a disordered graphitic material. From these data, it is expected that the formation of an ordered graphite should require a much higher pyrolysis temperature. However, the application of a higher temperature can cause a collapse of the porous structure [29, 30], diminishing its microporosity so its application in gas adsorption processes would not be beneficial. On the other hand, a broad band located between 2300 and 3000 cm^{-1} is also observed. This band is assigned to the overlapping of a band whose maximum is about 2650 cm^{-1}, which is attributed to 2D band due to the stacking of graphite layers [31]. In this region, another band with a maximum at 2850 cm^{-1} is detected. This band, denoted as D + D′, is ascribed to the presence of disordered carbon. The intensity of these overlapping bands is directly related to the ordering of graphitic structure. In the case of the biochars synthesized from wipe wastes, the formation of a graphitic material with low crystallinity implies that the 2D and D + D' bands display low intensity.

As the composition of the C-species is expected to vary according to the pyrolytic treatment, the ^{13}C NMR study analyses the evolution of the species formed after the pyrolytic treatment at different temperatures (Fig. 2). The analysis of the W-500 sample shows a main peak located about 126 cm^{-1} as well as a shoulder at 140 cm^{-1} [16,32]. These bands are ascribed to C-species with sp^2 hybridization [16,30]. The set of bands with maxima at about 40 cm^{-1} is assigned to the existence of aliphatic carbons, while the set of bands located at about 220 cm^{-1} are attributed to the presence of carbonyl bands [33]. The increase in temperature in the pyrolytic treatment causes a progressive decay of the intensity of the bands ascribed to carbonyl and aliphatic groups, confirming the removal of O-species and the aliphatic chains when the pyrolysis temperature increases. Thus, the band ascribed to C–C bonds with sp^2 hybridization is observed after the pyrolysis at 900 °C [16].

The study of the superficial chemical composition of the adsorbents was evaluated by XPS (Fig. 3 and Table 1). The analysis of the high-resolution C 1s core level spectra shows two contributions (Fig. 3A). The main contribution located about 284.8 eV is ascribed to the adventitious carbon, but it is also assigned to the C–C bond of the carbonaceous materials. In addition, a smaller contribution is observed at higher binding energy value (286.5 eV), which is attributed to C–O bonds.

The study of the O 1s core level spectra of the pyrolyzed wipe wastes shows two contributions located at 531.9 and 533.6 eV (Fig. 3B), which are attributed to the presence of -C-O and –C═O bonds, respectively. Interestingly, the ratio between the two oxygen species hardly changes despite the pyrolysis at higher temperature. Likewise, the analysis of the superficial atomic concentration of the obtained biochars shows that the C and O contents are very similar in all cases. Thus, C-content is in the range of 88–90% while the
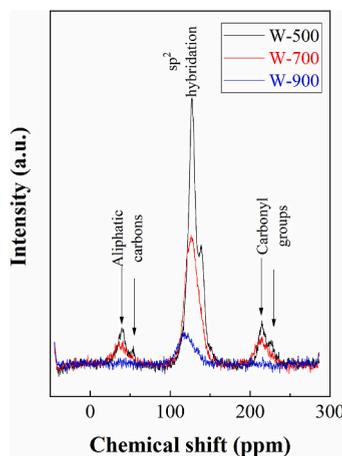

Fig. 2. ^{13}C MAS-NMR of the biochars synthesized at several temperatures.
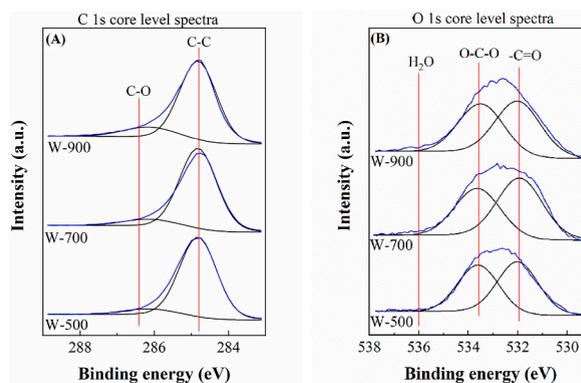
Fig. 3. C 1*s* (A) and O 1*s* (B) core level spectra of the biochars synthesized at several temperatures.

Table 1
Surface chemical analysis (in atomic concentration %) of the biochars synthesized at several temperatures.

Sample	Atomic concentrations (%)			
	C 1*s*	O 1*s*	Na 1*s*	Cl 2*p*
W-500	90.95	8.74	0.21	0.10
W-700	87.98	10.79	0.85	0.39
W-900	88.52	9.97	1.29	0.22

O-content is about 8–10%. In addition, small proportions of Na and Cl species have been also observed, probably due to the treatment with NaClO to remove the potential pathogens of the wipe wastes.

The study of the textural properties was carried out from CO_2-adsorption isotherms at 0 °C using the Dubinin-Radushkevich equation [34] (Table 2). Despite XPS data hardly showing changes in surface composition for pyrolysis carried out at different temperatures (Fig. 3), the textural properties are quite sensitive: higher pyrolysis temperatures lead to an increase in microporosity and the equivalent surface area. These results agree with those reported for other biochars obtained from cellulose residues [6,30] where the thermal treatment generates a physical activation forming microcavities in the biochars, which may have great potential to adsorb small molecules such as CO_2.

Finally, the morphology of the starting material and the biochar obtained at different temperatures was studied by SEM (Fig. 4). The study of the morphology of the wipes waste shows a fibrous structure with micrometric and homogeneous pores (Fig. 4A). The pyrolysis of the wipes at 500 °C (Fig. 4B) causes a collapse of such structure, thus obtaining a biochar with an elongated structure whose thickness is around 10 μm. Above this structure of interconnected fibers, smaller particles with poorly defined structures are also observed. A similar morphology is observed for the sample pyrolyzed at 700 °C (Fig. 4C). However, pyrolysis at a higher temperature (900 °C) provokes a collapse of the elongated structure leading to anisotropic particles (Fig. 4D). The study of the textural properties by CO_2-adsorption at 0 °C reported that the increase in temperature in the pyrolytic treatment caused an increase in microporosity. Considering these premises, the collapse of the homogeneous porous material observed in Fig. 4A is expected. However, this collapse must also be accompanied by the formation of microporosity in the sub-micrometer scale. This pore is so narrow that it cannot be detected by SEM or TEM. In fact, the pore diameter is so narrow, and the morphology of the cavities is so heterogeneous that it allows small molecules, such as CO_2, to be housed in its structure [23],[35]. The presence of this microporosity has been observed in any biochar studied although in residues of wipes it has not been studied yet. The formation of this microporosity increases as the temperature of the pyrolysis rises. However, the porosity of these biochars must be modulated since the use of an elevated temperature could result in a material with high porosity, increasing the microporosity and forming mesoporosity, which could cause a collapse of the porous structure.

Table 2
Textural properties of the biochars synthesized at several temperatures.

Sample	Limiting micropore capacity (mmol/g)	Limiting micropore volume (cm³/g)	Equivalent surface area (m²/g)	Density He-pycnometer (g/cm³)
W-500	4.23	0.174	434	1.47
W-700	5.53	0.227	566	1.80
W-900	6.30	0.285	645	1.94

These values were estimated from their CO_2-adsorption isotherms at 0 °C.
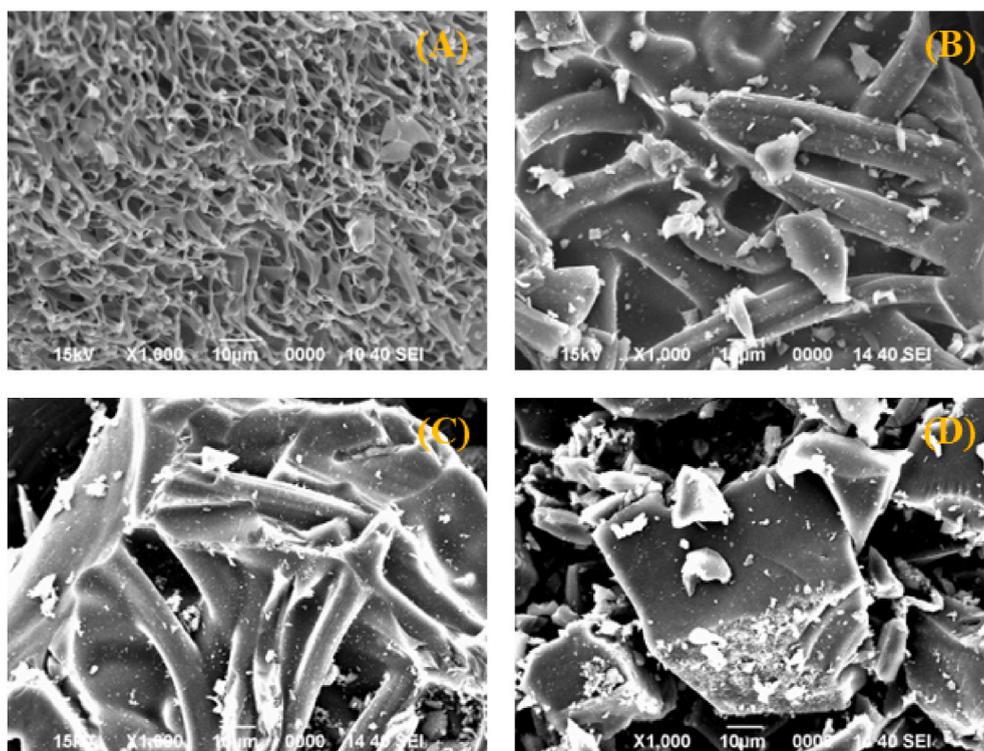
Fig. 4. SEM images of the raw wipes (A), W-500 (B), W-700 (C) and W-900 samples (D).

3.2. CO_2-adsorption isotherms

Once the biochars obtained from wipe wastes were characterized, the next step was the evaluation of the CO_2-adsorption capacity of the synthesized materials.

In the first adsorption study, the role of the temperature on the pyrolytic treatment was analyzed (Fig. 5). The adsorption isotherms show how an increase in temperature also causes a rise in the CO_2-adsorption capacity. Thus, the sample treated at 500 °C (W-500) only reaches a CO_2-adsorption of 1.35 mmol/g at 760 mm of Hg and 25 °C. The increase in pyrolysis temperature causes an improvement in the adsorption capacity of biochars, achieving a maximum value for the biochar pyrolyzed at 900 °C (W-900) of 2.53 mmol/g at 760 mm of Hg and 25 °C. These values are related to the microporosity of the adsorbent since the W-500 sample displayed the poorest textural properties, while the W-900 sample showed the highest microporosity (Table 2). The presence of a high micropore volume in the case of W-900 sample promotes hosting of a large amount of CO_2 molecules in micropores with undefined morphology. The morphology of these micropores can also be deduced from the profile of the CO_2 isotherms; W-500 sample shows nearly linear behavior with low adsorption capacity. However, a more pronounced curvature in the adsorption profile suggests that CO_2-adsorption is stronger due to the presence of a greater amount of narrow micropores. In fact, higher adsorption at lower pressures suggests a higher strength in the adsorbent-adsorbate interaction.
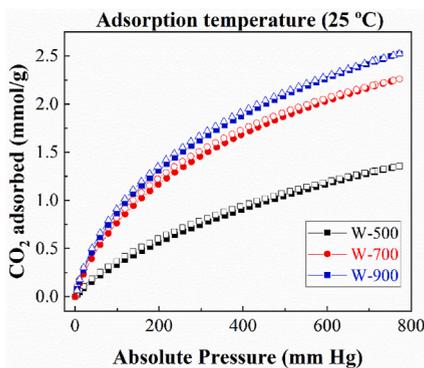

Fig. 5. CO_2-adsorption isotherms at 25 °C of the biochars synthesized at several temperatures.

The fit of the adsorption isotherms to the SIPS model (Table 3) confirms that the adsorbate-adsorbent strength increases for biochars produced at higher pyrolysis temperatures, as signaled by the parameter b. The simulation of the CO_2-adsorption capacity at infinite pressure would reach a maximum value of 4.39 mmol/g at 25 °C for the W-900 adsorbent. The heterogeneity of the adsorption process, defined by the n parameter, shows how this parameter decreases when the temperature of the pyrolytic treatment increases, suggesting that the adsorbent with high microporosity displays a more heterogeneous system that those adsorbents with low microporosity.

A comparison of the CO_2-adsorption capacity of the biochars obtained from wipe wastes with other adsorbents synthesized from lignocellulosic precursors is shown as follows. In a previous study, biochars synthesized from agricultural cellulosic wastes (cotton, wheat or linen) have shown an adsorption capacity of 2.5 mmol/g at a pressure of 760 mm Hg and a temperature of 25 °C [6]. Biochars obtained from chitosan, whereby a hydroxyl group is substituted by an amine group, reached a CO_2-adsorption capacity between 1.8 and 2.0 mmol/g, except for those materials prepared by freeze-drying method where a higher CO_2-adsorption capacity was observed due to the higher microporosity of the latter materials [30]. On the other hand, biochars synthesized from fruit shells such as coconut or almond achieve a CO_2-adsorption uptake between 2.5 and 2.7 at 760 mm of Hg at 25 °C [36–38]. Other authors synthesized biochars from olive stones attaining an adsorption capacity of 2.0 mmol/g at 760 mm of Hg at 25 °C [39]. These authors have also reported that activated carbon from sewage sludge only attains a CO_2-adsorption capacity of 0.3 mmol/g [39]. Considering the adsorption capacity of some biochars obtained from biomass of this study, the CO_2-adsorption capacity of the obtained biochars is similar other reported in the literature while these values are above to those reported by other wastes.

In the next analysis, the role of the adsorption temperature was evaluated (Fig. 6A, B and 6C). In all cases, it can be observed that an increase in the adsorption temperature gives rise to a drastic decrease in the CO_2 uptake, which is the expected behavior in physisorption. Other authors have reported that the adsorbents, where chemical adsorption sites predominate, show higher adsorption capacity when the temperature increases. This type of adsorption is typical for those adsorbents where a large amount of surface amino groups or alkaline-earth oxides appear on the surface [6,40]. Considering these premises, CO_2-adsorption using biochars synthesized from wipe wastes is governed by physical adsorption, since higher adsorption values are obtained at lower temperature [41,42]. Thus, the adsorbent with the highest CO_2-adsorption capacity (W-900) can achieve a value of 3.51 mmol/g at a pressure of 760 mm Hg and a temperature of 0 °C (Fig. 6C).

As the adsorption processes of the biochars synthesized at several temperatures of pyrolysis have been performed at several adsorption temperatures, it is possible to determine the isosteric heats of adsorption from the Clausius-Clapeyron equation (Fig. 7). This figure depicts how isosteric heats vary with the loading of CO_2 for each adsorbent. These data show how the adsorption heats of the samples differ at low q_m, obtaining the highest adsorption heat values for those biochars with higher microporosity. The higher isosteric heats of adsorption at "zero loading" are directly related to the large number of unoccupied pores, in such a way that the higher values are obtained for the sample with larger microporosity (W-900). The higher heat of adsorption for this adsorbent is ascribed to the presence of stronger van der Waals interactions due to its higher microporosity [43]. On the other hand, Fig. 7 also shows that the adsorption heat decreases with CO_2 loading for all samples, converging to similar adsorption heat values (25–26 kJ/mol) [43]. Under these conditions, nearly all the pores of the synthesized biochars are occupied and the adsorbent-adsorbate interactions tend to be weak for additional adsorbate loading. This implies that the adsorption heat values decrease, being very close to each other because of the chemical composition of the adsorbents is quite similar, as indicated by the characterization data (Fig. 3 and Table 1) [43]. The heat of adsorption at "zero loading" was compared for the biochar samples. The obtained results show a clear trend according to the pyrolysis temperature from $\Delta H_{q \to 0} = 31.8$ kJ/mol for the W-500 sample to $\Delta H_{q \to 0} = 39.5$ kJ/mol for the W-900 sample due to the increase of the microporosity of the biochar (Table 2).

To improve the adsorption capacity of the adsorbents synthesized from wipe wastes, activated carbons were synthesized from the biochar synthesized at 500 °C. For this purpose, this biochar was mixed with different proportions of KOH to promote an alkaline fusion in the biochar, followed by pyrolysis at 900 °C, thus generating an activated carbon with greater microporosity. Firstly, the textural properties of the obtained activated carbons were determined using the Dubinin-Radushkevich equation (Table 4) [34]. These data show how the microporosity increases when a low proportion of KOH (20 wt.%) is used to form the activated carbon, improving the microporosity from 0.258 cm^3/g for the W-900 sample to 0.305 cm^3/g for the W-900-20KOH sample. The use of higher KOH content to obtain activated carbons worsens the microporosity of the adsorbents since the microporosity decreases progressively, obtaining a micropore value of only 0.142 cm^3/g for the W-900-60KOH sample. These data point out that the use of a large amount of KOH can promote a higher microporosity in such a way that the structure of the porous material collapses, worsening its textural properties.

The study of the CO_2-adsorption capacity of these activated carbons synthesized with different proportions of KOH is compiled in Fig. 8. As was inferred from their textural properties (Table 4), the use of a lower proportion of KOH to form W-900-20KOH leads to an adsorbent with higher microporosity. This implies a higher adsorption capacity, obtaining a value of 2.95 mmol/g at 760 mm of Hg and 25 °C. However, this improvement is not observed when a higher amount of KOH in incorporated since the CO_2 capture capacity

Table 3
Sips model fitting parameters of the biochars synthesized at several temperatures.

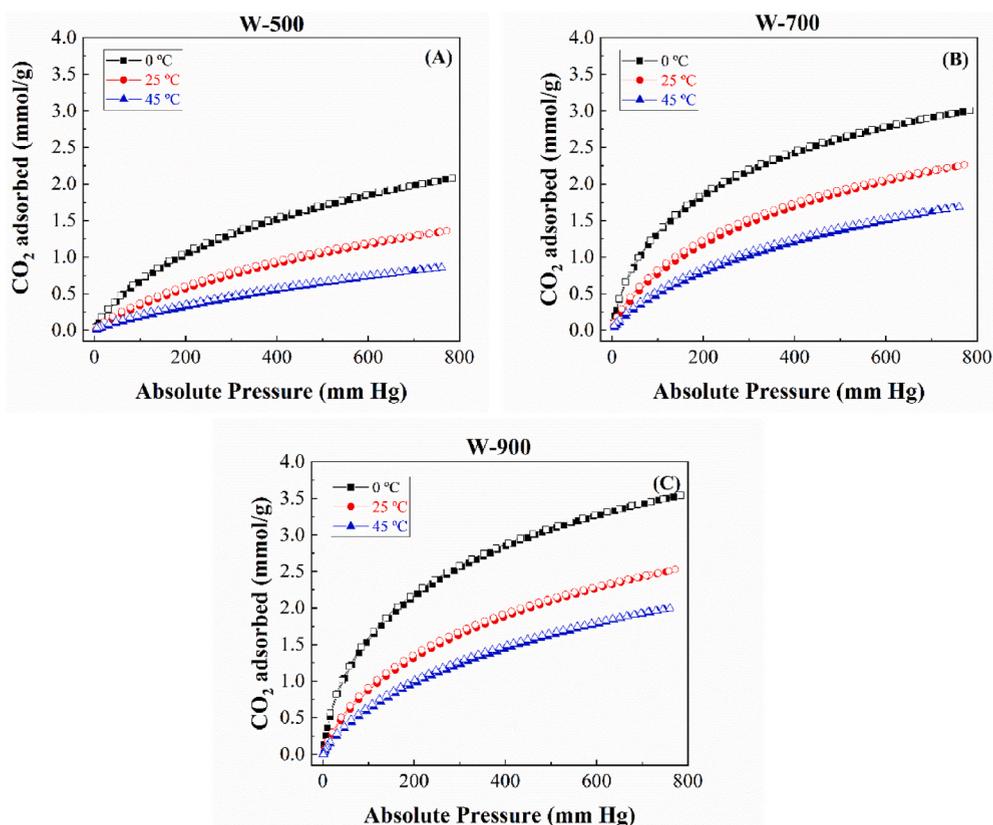| Sample	q_m (mmol/g)	b (mm Hg^{-1})	n
W-500	2.32	$1.55 \cdot 10^{-3}$	0.84
W-700	4.24	$2.04 \cdot 10^{-3}$	0.76
W-900	4.39	$1.79 \cdot 10^{-3}$	0.82

Fig. 6. CO_2-adsorption isotherms at 0, 25 and 45 °C of the biochars synthesized at several temperatures.
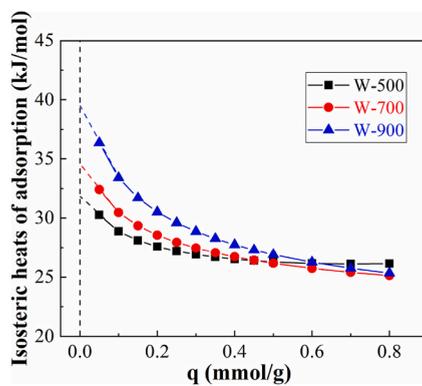

Fig. 7. Adsorption heat as a function of q_{CO_2} adsorbed for the biochars synthesized at several temperatures.

Table 4
Textural properties of the activated carbons synthesized with several KOH proportion.

Sample	Limiting micropore capacity (mmol/g)	Limiting micropore volume (cm³/g)	Equivalent surface area (m²/g)	Density He-pycnometer (g/cm³)
W-900	6.30	0.285	645	1.94
W-900-20KOH	7.44	0.305	762	2.13
W-900-40KOH	5.79	0.240	599	1.82
W-900-60KOH	3.47	0.142	355	1.60

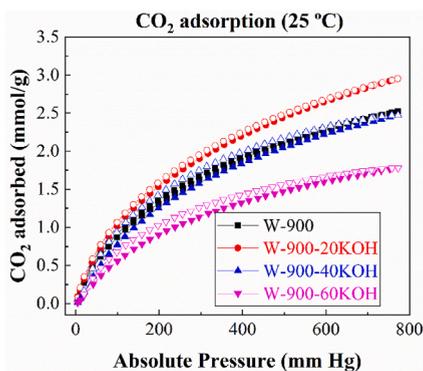These values were estimated from their CO_2-adsorption isotherms at 0 °C.

Fig. 8. CO_2-adsorption isotherms at 25 °C of the activated carbons synthesized from several KOH proportions.

decreases progressively to a value of 1.77 mmol/g at 760 mm of Hg and 25 °C. The decrease in the adsorption capacity has been attributed to an increase in porosity generated by the large amount of KOH in such a way that its structure cannot support it, causing a partial collapse of the adsorbent and implying a decrease in its capacity to capture CO_2. The adsorbents were fitted to the SIPS model (Table 5) which shows how the interaction adsorbate-adsorbent increases when a higher amount of KOH is added to synthesize the activated carbons, although the addition of a high proportion of KOH causes a collapse in the structure. In the same way, the fit of the activated carbons to the SIPS model also shows the n parameter approaches unity when the activated carbons are synthesized with high levels of KOH. This implies that adsorption takes place in more homogeneous systems.

The study of the CO_2-adsorption capacity of the wipe wastes pyrolyzed are compared with other data reported in the literature for other pyrolyzed waste (Table 6). From these data, it can be observed how the CO_2-adsorption capacity values differ between them. However, several parameters should be considered as the starting material, the physical or chemical activation of the carbon as well as the pressure of the adsorption process.

As stated above, the CO_2 capture is a key step in the CCS process due to its high cost in many cases. Thus, it is necessary the synthesis and development of low-cost adsorbents to make the process economically sustainable [13]. However, another parameter to be considered is the use of highly selective adsorbents towards CO_2, avoiding competence for the same adsorption sites. One of these cases is the selective adsorption of CO_2 with respect to N_2 in the flue gases (Fig. 9). Thus, the study of the CO_2-adsorption capacity of the W-900 sample showed a value of 2.53 mmol/g at 760 mm of Hg and 25 °C. However, the N_2-adsorption was much more limited since the adsorption value is only of 0.19 mmol/g after similar adsorption conditions (Fig. 9A). The analysis of the adsorption profiles shows how the N_2-adsorption is linear while the profile of the CO_2-adsorption displays a pronounced curvature. This implies that the CO_2-adsorption process on the biochar is stronger than that observed when N_2 is adsorbed. In this sense, previous authors have pointed out that the greater quadrupole moment of the CO_2-molecule promotes a stronger adsorption with narrow pore adsorbents [54].

The analysis of the selective CO_2/N_2-adsorption (Fig. 9B) shows how W-900 sample displays higher CO_2 selectivity at lower pressure. This confirms the higher CO_2-adsorption capacity at lower pressure, which implies a stronger interaction of the biochar with the CO_2 molecules due to its higher quadrupole moment. The CO_2/N_2 ratio decreases drastically at low pressure; however, the decrease in the CO_2/N_2 ratio is more progressive as the pressure increases, reaching a CO_2/N_2 ratio of 14 at 760 mm of Hg at 25 °C.

In the same the separation of CO_2 to H_2 can also be interesting in the H_2-purification processes since the water gas shift reaction forms CO_2 and H_2 as products. The analysis of the CO_2 and H_2-adsorption isotherms at 25 °C, compiled in Fig. 10A, shows how the H_2-adsorption is very low, about 0.04 mmol/g at 760 mm of Hg, in comparison to the CO_2-adsorption. The low quadrupole moment as well as the small dimensions of H_2-molecules prevent H_2-adsorption on a microporous structure. The analysis of the CO_2/H_2 (Fig. 10B), shows how the biochar is highly selective towards CO_2 at low pressure, obtaining a maximum value close to 1850. This suggests that the strength of interaction between CO_2 and biochar is much stronger than that observed when H_2 is used as adsorbate. In fact, the CO_2/H_2 ratio is higher than that observed for CO_2/N_2 in Fig. 9B, which confirms that the low quadrupole moment together with the small dimensions of H_2 molecule makes its adsorption negligible at room temperature. The study of the CO_2/H_2 ratio at higher pressure shows a decrease in this ratio until it is progressively stabilized at higher pressures, achieving a value of 66 at 760 mm of Hg and 25 °C. From these data, it can be inferred that the biochars obtained from wipe waste can be considered for H_2 purification processes.

Despite its isotherm showed a low H_2-adsorption capacity at room temperature, a study at lower temperature could allow the use this biochar in H_2-storage processes (Fig. 11). The profile of this isotherm differs to that carried out at 25 °C (Fig. 10A). Thus, the isotherm carried out at −196 °C presents a greater curvature, increasing its adsorption capacity at lower pressures. This implies that the interaction between biochar and H_2-molecules becomes significant at low temperatures. Furthermore, the analysis of the H_2-isotherms at different temperatures shows that adsorption is favored at low temperatures, confirming that the adsorption in these biochars takes place through a physical process. This assumes that the H_2-captured in the W-900 biochar is 1.3% of its weight so the material could be also to H_2-storage at low temperature. The values are higher to that reported for biochars obtained from agrochemical wastes under similar synthetic and adsorption conditions [6].

Finally, the H_2 and CO_2-adsorption processes can be considered physical because biochar has a highly porous structure with a large amount of micropores. The physical mechanism of CO_2 or H_2-adsorption on biochar involves gas molecules diffusing into these pores

Table 5
Sips model fitting parameters of the activated carbons synthesized with several KOH proportion.

Sample	q_m (mmol/g)	b (mm Hg^{-1})	N
W-900	4.39	$1.79 \cdot 10^{-3}$	0.82
W-900-20KOH	5.49	$1.51 \cdot 10^{-3}$	0.80
W-900-40KOH	4.06	$2.06 \cdot 10^{-3}$	0.93
W-900-60KOH	2.82	$2.23 \cdot 10^{-3}$	0.95

Table 6
CO_2-adsorption capacity at 25 °C and different pressures for carbonaceous materials reported in the literature.

Carbon source	CO_2-adsorption capacity (mmol/g)	Reference
Wipe waste	2.95	This work
Waste CDs and DVDs	3.30	[44]
Rice husk	3.71	[45]
Starch	3.84	[46]
Packaging waste	4.20	[47]
Bean dreg	4.24	[48]
Pine nutshell	5.00	[49]
Coconut shell	5.00	[50]
Walmut shell	5.17	[51]
Argan fruit Shell	5.63	[52]
Common Polypody	5.67	[53]
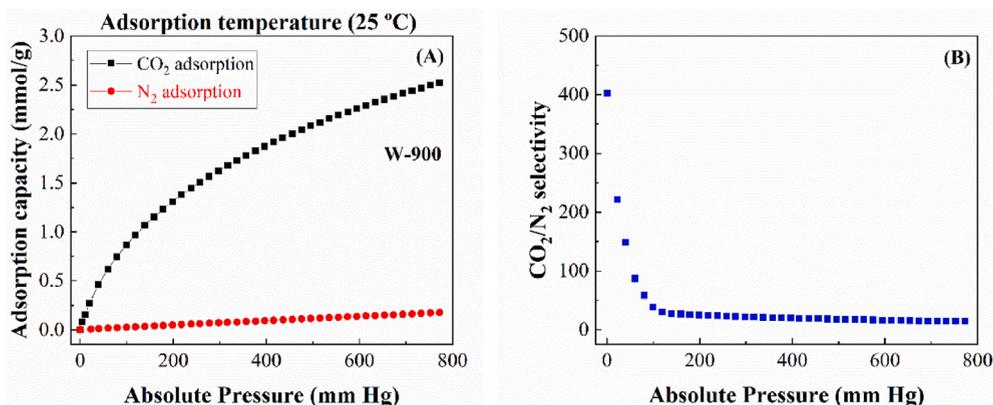
Fig. 9. CO_2 and N_2-adsorption isotherms (A) and CO_2/N_2 ratio (B) at 25 °C for the W-900 sample. (The CO_2/N_2 ratio was determined from its pure isotherms at 25 °C).
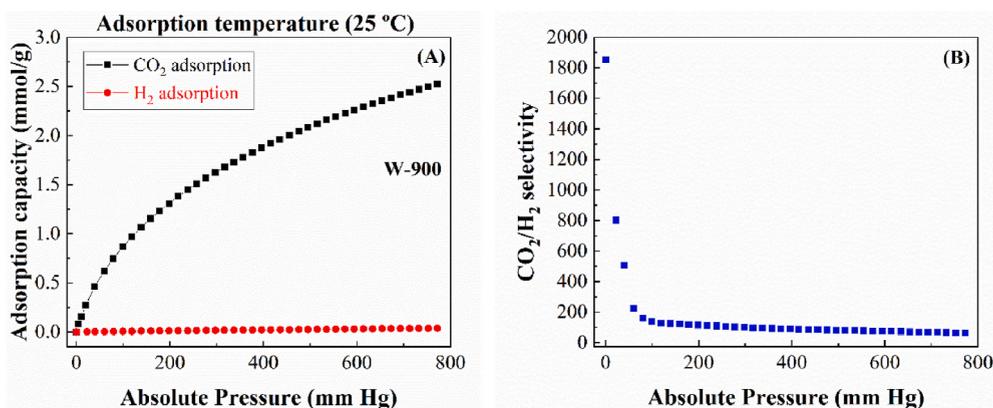
Fig. 10. CO_2 and H_2-adsorption isotherms (A) and CO_2/H_2 ratio (B) at 25 °C for the W-900 sample. (The CO_2/H_2 ratio was determined from its pure isotherms at 25 °C).
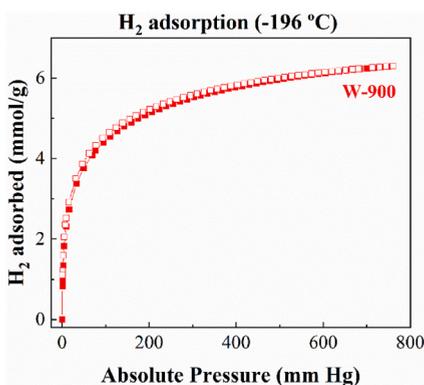
Fig. 11. H$_2$-adsorption isotherm at $-196\ ^\circ$C for the W-900 sample.

and becoming trapped on the internal surfaces. The large microporosity provides more sites for CO_2 or H_2 molecules to interact with the biochar, leading to higher adsorption capacity. The higher adsorption capacity for the CO_2 molecules is mainly ascribed to their higher quadrupole moment, which promotes a stronger interaction of the microporous adsorbent. On the other hand, the presence of a chemical interaction should not be ruled out. The analysis of the biochars by XPS reported the presence of oxygenated species (Table 1 and Fig. 3), which can also form weak chemical bonds with CO_2 molecules.

4. Conclusions

Biochars have been successfully synthesized from waste wipes collected from sewage treatment plants. After disinfection, drying and pyrolysis treatment, biochars were obtained, some of which were further activated with KOH. These materials were selected as adsorbents for CO_2 capture. The results obtained reported that an increase in pyrolysis temperature leads to increased microporosity. The increase in microporosity gives rise to materials with a greater capacity to capture CO_2 by physical adsorption, achieving a value of 2.53 mmol/g at 25 $^\circ$C and a pressure of 760 mm of Hg for the sample treated at 900 $^\circ$C. This adsorbent also reported interesting results in purification processes since the adsorbent is highly selective in CO_2/N_2 and CO_2/H_2 mixtures thus showing promise of application in CO_2 capture from flue gas and H_2-purification, respectively.

The CO_2-adsorption capacity was improved by chemical activation with KOH, leading to activated carbons with higher adsorption capacity since the addition promotes the formation of higher proportion of micropores. However, the formation of an excess of microporosity has an adverse effect since the presence of a high proportion of micropores can cause a collapse of the porous structure, leading to an adsorbent with lower microporosity in such a way these materials display lower CO_2-adsorption capacity.

Author contribution statement

J.A. Cecilia: Conceived and designed the experiments; Performed the experiments; Analyzed and interpreted the data; Wrote the paper.

E. Vilarrasa-García: Performed the experiments; Analyzed and interpreted the data; Wrote the paper.

D.C.S. Azevedo: Analyzed and interpreted the data; Contributed reagents, materials, analysis tools or data.

A. Vílchez-Cózar: Performed the experiments.

A. Infantes-Molina: Analyzed and interpreted the data.

D. Ballesteros-Plata: Performed the experiments; Wrote the paper.

I. Barroso-Martín: Analyzed and interpreted the data; Wrote the paper.

E. Rodríguez-Castellón: Contributed reagents, materials, analysis tools or data; Wrote the paper.

Declaration of competing interest

The authors declare the following financial interests/personal relationships which may be considered as potential competing interests.

Acknowledgments

References

[1] https://www.nacwa.org/docs/default-source/resources---public/govaff-3-cost_of_wipes-1.pdf?sfvrsn=b535fe61_2.

[2] https://zerowasteeurope.eu/wp-content/uploads/2019/12/bffp_single_use_menstrual_products_baby_nappies_and_wet_wipes.pdf.

[3] Y. Liao, B. Op de Beeck, K. Thielemans, T. Ennaert, J. Snelders, M. Dusselier, C.M. Courtin, B.F. Sels, The role of pretreatment in the catalytic valorization of cellulose, Mol. Catal. 487 (2020), 110883, https://doi.org/10.1016/j.mcat.2020.110883.

[4] Y. Wu, H. Wang, J. Peng, M. Ding, Advances in catalytic valorization of cellulose into value-added chemicals and fuels over heterogeneous catalysts, Catal. Today 408 (2023) 92–110, https://doi.org/10.1016/j.cattod.2022.08.012.

[5] V.K.Gupta Suhas, P.J.M. Carrott, R. Singh, M. Chaudhary, S. Kushwaha, Cellulose: a review as natural, modified and activated carbon adsorbent, Bioresour. Technol. 216 (2016) 1066–1076, https://doi.org/10.1016/j.biortech.2016.05.106.

[6] N. Chouikhi, J.A. Cecilia, E. Vilarrasa-García, L. Serrano-Cantador, S. Besghaier, M. Chlendi, M. Bagane, E. Rodríguez-Castellón, Valorization of agricultural waste as a carbon materials for selective separation and storage of CO_2, H_2 and N_2, Biomass Bioenergy 155 (2021), 106297, https://doi.org/10.1016/j.biombioe.2021.106297.

[7] T. Xie, K.R. Reddy, C. Wang, E. Yargicoglu, K. Spokas, Characteristics and applications of biochar for environmental remediation: a review, Crit. Rev. Environ. Sci. Technol. 45 (2015) 939–969, https://doi.org/10.1080/10643389.2014.924180.

[8] R.P. Lopes, D. Astruc, Biochar as a support for nanocatalysts and other reagents: Recent advances and applications, Coord. Chem. Rev. 426 (2021), 213585, https://doi.org/10.1016/j.ccr.2020.213585.

[9] C. Kalinke, P.R. de Oliveira, J.A. Bonacin, B.C. Janegitz, A.S. Mangrich, L.H. Marcolino-Junior, M.F. Bergamini, State-of-the-art and perspectives in the use of biochar for electrochemical and electroanalytical applications, Green Chem. 23 (2021) 5272–5301, https://doi.org/10.1039/D1GC00843A.

[10] R. Das, S.N. Panda, Preparation and applications of biochar based nanocomposite: a review, J. Anal. Appl. Pyrolysis 167 (2022), 105691, https://doi.org/10.1016/j.jaap.2022.105691.

[11] Y. Chen, X. Zhang, W. Chen, H. Yang, H. Chen, The structure evolution of biochar from biomass pyrolysis and its correlation with gas pollutant adsorption performance, Bioresource Technol 246 (2017) 101–109, https://doi.org/10.1016/j.biortech.2017.08.138.

[12] S. Guo, Y. Li, Y. Wang, L. Wang, Y. Sun, L. Liu, Recent advances in biochar-based adsorbents for CO_2 capture, Carbon Capture Sci. Technol. 4 (2022), 100059, https://doi.org/10.1016/j.ccst.2022.100059.

[13] M. Pera-Titus, Porous inorganic membranes for CO_2 capture: present and prospects, Chem. Rev. 114 (2014) 1413–1492, https://doi.org/10.1021/cr400237k.

[14] E.I. Koytsoumpa, C. Bergins, E. Kakaras, The CO_2 economy: review of CO_2 capture and reuse technologies, J. Supercrit. Fluids 132 (2018) 3–16, https://doi.org/10.1016/j.supflu.2017.07.029.

[15] S. Perathoner, K.M. van Geem, G.B. Marin, G. Centi, Reuse of CO_2 in energy intensive process industries, Chem. Commun. 57 (2021) 10967–10982, https://doi.org/10.1039/D1CC03154F.

[16] N. Chouikhi, J.A. Cecilia, E. Vilarrasa-García, S. Besghaier, M. Chlendi, F.I. Franco-Duro, E. Rodríguez-Castellón, CO_2 adsorption of materials synthesized from clay minerals: a review, Minerals 9 (2019) 514, https://doi.org/10.3390/min9090514.

[17] J.A. Cecilia, E. Vilarrasa-García, C.L. Cavalcante Jr., D.C.S. Azevedo, F. Franco, E. Rodríguez-Castellón, Evaluation of two fibrous clay minerals (sepiolite and palygorskite) for CO_2 capture, J. Environ. Chem. Eng. 6 (2018) 4573–4587, https://doi.org/10.1016/j.jece.2018.07.001.

[18] S. Kumar, R. Srivastava, J. Koh, Utilization of zeolites as CO_2 capturing agents: advances and future perspectives, J. CO_2 Util. 41 (2020), 101251, https://doi.org/10.1016/j.jcou.2020.101251.

[19] Z. Zhang, Y. Xiao, B. Wang, Q. Sun, H. Liu, Waste is a misplayed resource: synthesis of zeolites from fly ash for CO_2 capture, Energy Proc. 114 (2017) 2537–2544, https://doi.org/10.1016/j.egypro.2017.08.036.

[20] J.A. Cecilia, E. Vilarrasa-García, R. Morales-Ospino, E. Finocchio, G. Busca, K. Sapag, J. Villaroel-Rocha, M. Bastos-Neto, D.C.S. Azevedo, E. Rodríguez-Castellón, Kaolinite-based zeolites synthesis and their application in CO_2 capture processes, Fuel 320 (2022), 123953, https://doi.org/10.1016/j.fuel.2022.123953.

[21] M.R. Ketabchi, S. Babamohammadi, W.G. Davies, M. Gorbounov, S.M. Soltani, Latest advances and challenges in carbon capture using bio-based sorbents: a state-of-the-art review, Carbon Capture Sci. Technol. 6 (2023), 100087, https://doi.org/10.1016/j.ccst.2022.100087.

[22] A.A. Ogungbenro, D.V. Quang, K. Al-Ali, M.R.M. Abu-Zahra, Activated carbon from date seed for CO_2 capture applications, Energy Proc. 114 (2017), https://doi.org/10.1016/j.egypro.2017.03.1370, 2313-2221.

[23] J. Serafin, B. Dziejarski, Activated carbons-preparation, characterization and their application in CO2 capture: a review, Environ. Sci. Pollut. Res. (2023), https://doi.org/10.1007/s11356-023-28023-9. In press.

[24] J. Serafin, B. Dziejarski, X. Vendrell, K. Kielbasa, B. Michalkiewicz, Biomass waste fern leaves as a material for a sustainable method of activated carbon production for CO_2 capture, Biomass Bioenergy 175 (2023), 106880, https://doi.org/10.1016/j.biombioe.2023.106880.

[25] J. Gautam, S. Serafin, B. Vikram, S. Dziejarski, Sahoo. An environmentally friendly synthesis method of activated carbons based on subabul (Leucaena leucocephala) sawdust waste for CO_2 adsorption, J. Clean. Prod. 412 (2023), 137406, https://doi.org/10.1016/j.jclepro.2023.137406.

[26] G. Singh, K.S. Lakhi, S. Sil, S.V. Bhosale, I. Kim, K. Albahily, A. Vinu, Biomass derived porous carbon for CO_2 capture, Carbon 148 (2019) 164–186, https://doi.org/10.1016/j.carbon.2019.03.050.

[27] J.A. Cecilia, E. Vilarrasa-García, N. Chouikhi, R. Morales-Ospino, S. Besghaier, M. Chlendi, M. Bagane, M. Bastos-Neto, D.C.S. Azevedo, E. Rodríguez-Castellón, Activated carbons synthesized from sucrose using porous clay heterostructures as template for CO_2 adsorption, Sustain. Chem. Climate Action. 1 (2022), 100006, https://doi.org/10.1016/j.scca.2022.100006.

[28] S. Kou, L.M. Peters, M.R. Mucalo, Chitosan: a review of sources and preparation methods, Int. J. Biol. Macromol. 169 (2021) 85–94, https://doi.org/10.1016/j.ijbiomac.2020.12.005.

[29] X Zhu, M. Sun, X. Zhu, W. Guo, Z. Luo, W. Cai, X. Zhu. Molten salt shielded pyrolysis of biomass waste: Development of hierarchical biochar, salt recovery, CO_2 adsorption. Fuel 334 (334) 126565. https://doi.org/10.1016/j.fuel.2022.126565.

[30] I. Barroso-Martín, J.A. Cecilia, E. Vilarrasa-García, D. Ballesteros-Plata, C.P. Jiménez-Gómez, A. Vílchez-Cózar, A. Infantes-Molina, E. Rodríguez-Castellón, Modification of the textural properties of chitosan to obtain biochars for CO_2-capture processes, Polymers 14 (2022) 5240, https://doi.org/10.3390/polym14235240.

[31] R.J. Nemanich, S.A. Dolin, First- and second-order Raman scattering from finitesize crystals of graphite, Phys. Rev. B 20 (1979) 392–401, https://doi.org/10.1103/PhysRevB.20.392.

[32] A.C. Ferrari, D.M. Basko, Raman spectroscopy as a versatile tool for studying the properties of graphene, Nat. Nanotechnol. 8 (2013) 235–246, https://doi.org/10.1038/nnano.2013.46.

[33] Y.S.S. Al-Faiyz, CPMAS ^{13}C NMR characterization of humic acids from composted agricultural Saudi waste, Arabian J. Chem. 10 (2017) S839–S853, https://doi.org/10.1016/j.arabjc.2012.12.018.

[34] M.M. Dubinin, Fundamentals of the theory of adsorption in micropores of carbon adsorbents: characteristics of their adsorption properties and microporous structures, Carbon 27 (1989) 457–467, https://doi.org/10.1016/0008-6223(89)90078-X.

[35] A. Tomczyk, Z. Sokolowska, P. Boguta, Biochar physicochemical properties: pyrolysis temperature and feedstock kind effects, Rev. Environ. Sci. Biotechnol. 19 (2020) 191–215, https://doi.org/10.1007/s11157-020-09523-3.

[36] G. Chandrasekar G, W.J. Son, W.S. Ahn, Synthesis of mesoporous materials SBS-15 and CMK-3 from fly ash and their application for CO_2 adsorption, J. Porous Mater. 16 (2009) 545–551, https://doi.org/10.1007/s10934-008-9231-x.

[37] H. Yang, M. Gong, Y. Chen, Preparation of activated carbons and their adsorption properties for greenhouse gases: CH_4 and CO_2, J. Nat. Gas Chem. 20 (2011) 460–464, https://doi.org/10.1016/S1003-9953(10)60232-0.

[38] M.G. Plaza, C. Pevida, C.F. Martin, J. Fermoso, J.J. Pis, F. Rubiera, Developing almond shell-derived activated carbons as CO_2 adsorbents, Sep. Purif. Technol. 71 (2010) 102–106, https://doi.org/10.1016/j.seppur.2009.11.008.

[39] M.G. Plaza, C. Pevida, B. Arias, M.D. Casal, C.F. Martin, J. Fermoso, F. Rubiera, J.J. Pis, Different approaches for the development of low-cost CO_2 adsorbents, J Environ Eng 135 (2009) 426–432, https://doi.org/10.1061/(ASCE)EE.143-7870.0000009.

[40] E. Vilarrasa-García, J.A. Cecilia, D.C.S. Azevedo, C.L. Cavalcante Jr., E. Rodríguez-Castellón, Evaluation of porous clay heterostructures modified with amine species as adsorbent for the CO_2 capture, Micropor. Mesopor. Mater. 249 (2017) 25–33, https://doi.org/10.1016/j.micromeso.2017.04.049.

[41] L. Hauchhum, P. Mahanta, Kinetic, thermodynamic and regeneration studies for CO_2 adsorption onto activated carbon, Int. J. Adv. Mech. Eng. 4 (2014) 27–32.

[42] B. Guo, L. Chang, K. Xiel, Adsorption of carbon dioxide on activated carbon, J. Nat. Gas Chem. 15 (2006) 223–229, https://doi.org/10.1016/S1003-9953(06)60030-3.

[43] V.K. Singh, E.A. Kumal, Experimental investigation and thermodynamic analysis of CO_2 adsorption on activated carbons for cooling system, J. CO_2 Util. 17 (2017) 290–304, https://doi.org/10.1016/j.jcou.2016.12.004.

[44] J. Choma, M. Marszewski, L. Osuchowski, J. Jagiello, A. Dziura, M. Jaroniec, Adsorption properties of activated carbons prepared from waste CDs and DVDs, ACS Sustain. Chem. Eng. 3 (2015) 733–742, https://doi.org/10.1021/acssuschemeng.5b00036.

[45] D. Li, T. Ma, R. Zhang, Y. Tian, Y. Qiao, Preparation of porous carbons with high low-pressure CO2 uptake by KOH activation of rice husk char, Fuel 139 (2015) 68–70, https://doi.org/10.1016/j.fuel.2014.08.027.

[46] A. Alabadi, S. Razzaque, Y. Yang, S. Chen, B. Tan, Highly porous activated carbon materials from carbonized biomass with high CO_2 capturing capacity, Chem. Eng. J. 281 (2015) 606–612, https://doi.org/10.1016/j.cej.2015.06.032.

[47] M. Idrees, V. Rangari, S. Jeelani, Sustainable packaging waste-derived activated carbon for carbon dioxide capture, J. CO_2 Util. 26 (2018) 380–387, https://doi.org/10.1016/J.JCOU.2018.05.016.

[48] W. Xing, C. Liu, Z. Zhou, L. Zhang, J. Zhou, S. Zhuo, Z. Yan, H. Gao, G. Wang, S.Z. Qiao, Superior CO_2 uptake of N-doped activated carbon through hydrogen-bonding interaction, Energy Environ. Sci. 5 (2012) 7323, https://doi.org/10.1039/c2ee21653a.

[49] S. Deng, H. Wei, T. Chen, B. Wang, J. Huang, G. Yu, Superior CO_2 adsorption on pine nut shell-derived activated carbons and the effective micropores at different temperatures, Chem. Eng. J. 253 (2014) 46–54, https://doi.org/10.1016/j.cej.2014.04.115.

[50] J. Chen, J. Yang, G. Hu, X. Hu, Z. Li, S. Shen, M. Radosz, M. Fan, Enhanced CO_2 capture capacity of nitrogen-doped biomass-derived porous carbons, ACS Sustain. Chem. Eng. 4 (2016) 1439–1445, https://doi.org/10.1021/acssuschemeng.5b01425.

[51] J. Serafin, B. Dziejarski, O.F. Cruz Junior, J. Srensscek-Nazzal, Design of highly microporous activated carbons based on walnut shell biomass for H_2 and CO_2 storage, Carbon 201 (2023) 633–647, https://doi.org/10.1016/j.carbon.2022.09.013.

[52] O. Boujibar, A. Souikny, F. Ghamouss, O. Achak, M. Dahbi, T. Chafik, CO_2 capture using N-containing nanoporous activated carbon obtained from argan fruit shells, J. Environ. Chem. Eng. 6 (2018) 1995–2002, https://doi.org/10.1016/J.JECE.2018.03.005.

[53] J. Serafin, K. Kiełbasa, B. Michalkiewicz, The new tailored nanoporous carbons from the common polypody (Polypodium vulgare): the role of textural properties for enhanced CO_2 adsorption, Chem. Eng. J. 429 (2022), 131751, https://doi.org/10.1016/j.cej.2021.131751.

[54] S. Furmaniak, P. Kowalczyk, A.P. Terzyk, P.A. Gauden, P.J.F. Harris, Synergetic effect of carbon nanopore size and surface oxidation on CO_2 capture from CO_2/CH_4 mixtures, J. Colloid Interf. Sci. 397 (2013) 144–153, https://doi.org/10.1016/j.jcis.2013.01.044.